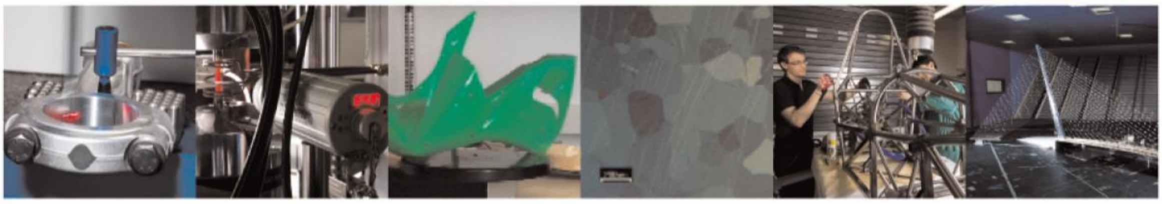

A simulation method to estimate task-specific uncertainty in 3D microscopy

Moroni, Giovanni; Syam, Wahyudin P.; Petrò, Stefano

A simulation method to estimate task-specific uncertainty in 3D Microscopy

Giovanni Moroni[1,2], Wahyudin P. Syam[3], and Stefano Petrò[2]
[1] School of Mechanical Engineering, Tongji University, Cao An Road, 201804 Shanghai, P.R. of China
[2] Mechanical Engineering Department, Politecnico di Milano, Via La Masa 1, 20156 Milan, Italy
[3] Manufacturing Metrology Team, Faculty of Engineering, The University of Nottingham, NG7 2RD, Nottingham, UK

Corresponding author: Wahyudin P. Syam (Wahyudin.syam@nottingham.ac.uk)

Abstract:
Traceability in micro-metrology requires an infrastructure of accredited metrology institutes, effective performance verification procedures, and task specific uncertainty estimation. Focusing on the latter, this paper proposes an approach for the task specific uncertainty estimation based on simulation for a generic 3D microscope. The proposed simulation approach is based on the identification and successive parameter estimation of an empirical model of the measured points. The model simulates the probing error based on a Gaussian process model, thus including the correlation among close points. Parameters for the error simulation are estimated by a deep analysis of error sources of the 3D microscope. Validations of the proposed simulation approach are carried out in the case of focus variation microscopy (FVM), considering several case studies. The procedure proposed in the ISO/TS 15530-4 standard are applied for validation.

Keywords: Uncertainty, 3D microscopy, geometrical metrology, micro-metrology, ISO/TS 15530-4, focus-variation.

1. Introduction

Micro-engineered components are important since they can integrate functions and intelligence into products [1]. These products need micro-geometrical metrology to verify their compliance to tolerances. Coordinate measuring systems (CMSs), being suitable for micro-geometrical metrology are in most cases non-contact (optical) instruments, due to their flexibility in accessing the surface of parts, elimination of the risk of damaging small and delicate micro features and fast data acquisition rate [2]. Among the others, 3D microscopy (3DM) seems very promising and already counts a lot of industrial applications, particularly in the field of surface analysis. 3DM gathers technique like coherence scanning interferometry, phase shifting interferometry, confocal scanning microscopy, confocal chromatic microscopy, digital holography, and focus variation microscopy. Most 3DM techniques are based on the sequential acquisition of images of the sample, while changing the distance between the sample and the objective lens.

1.1 Measurement traceability and uncertainty

Regardless of the considered measuring instruments, traceability of measurements is very important for a reliable measurement result in the case of micro-geometrical metrology as well. Traceability requires not only periodical instrument performance verification to check if measuring instruments behave as stated by the manufacturer or according to some predefined performance index, but also measurement uncertainty must be stated to guarantee measurement comparability [3]. The subject of performance verification has been addressed by the authors in previous papers [4, 5]: this paper addresses the problem of the uncertainty estimation.

The main reference for measurement uncertainty estimation is the "Guide to the expression of uncertainty in measurement" (GUM) [6]. According to the GUM, when a final measurement result comes from several distinct measurement data processes, the uncertainty is derived based on the propagation of the uncertainty from each uncertainty contributor along the data processing chain, thus GUM requires a closed form mathematical model of the measurement. In addition, for coordinate metrology, measurement uncertainty is "task-specific" [7], i.e. a single measuring instrument can perform several different measurement tasks with different measuring strategies, which are characterized by a different uncertainty [8]; hence the GUM method is difficult to apply.

The ISO 15530-3 [9] and ISO/TS 15530-4 [10] standards propose alternative methods to effectively estimate the measurement uncertainty for coordinate metrology. The ISO 15530-3 method needs expensive calibrated artifacts; hence it is not suitable when a product has many variants, as it would require many different calibrated artifacts, or when small production volume cannot justify the cost of a calibrated artifact. The ISO/TS 15530-4 simulation method seems more promising in the case of high product or high demand variability. The main drawback of the simulation method is its computational intensity [11], but the continuous reduction of computational costs should reduce this issue.

1.2 Simulation approaches

A simulation-based approach seems to be the most promising solution to estimate a task-specific measurement uncertainty, especially for optical-distance sensor instruments, as suggested by Evans [11] in the case of interferometry. Baldwin et al. [9] used a simulation approach to estimate the uncertainty in tactile-CMM measurement. They simulated CMM geometric errors and incorporated them in the kinematic model of the CMM, so that the nominal position of points could be modified. Kruth et al. [12] proposed a similar approach, with addition of part form deviation as an uncertainty source. Cheung et al. [13] also used a similar approach to estimate the uncertainty in the case of free-form surface measurements. All these simulation approaches neglect the presence of spatial correlations among the sampled points.

In general, a simulation approach relies on a point perturbation process (an error simulator) generating a perturbation of a reference cloud of points, as shown in Figure 1. Detailed explanation of the framework applied to CMMs was described by Trapet and Waldele [14]. The scheme consists of two paths, the first one (Figure 1: black arrow) estimates a measurement result *Y*, while the second one (Figure 1: red arrow) estimates the measurement uncertainty *U*. The first path is explained as follows: a point cloud is obtained by the selected measuring system using a defined measuring strategy. This point cloud is then processed to calculate the measurement result *Y*. The second path starts from the same sampled point cloud. A point perturbation process by measurement error simulation is applied to the original point cloud. The perturbed point cloud is processed by the same numerical algorithm that gathered to the measurement result and the results are stored. The simulation of the error is repeated for an adequate number of times (usually a few thousand) and the simulated measurement results are stored. The estimated uncertainty u_{sim} ($U = 2\ u_{sim}$) of a measurement is the sample standard deviation of the stored results from the simulation runs.

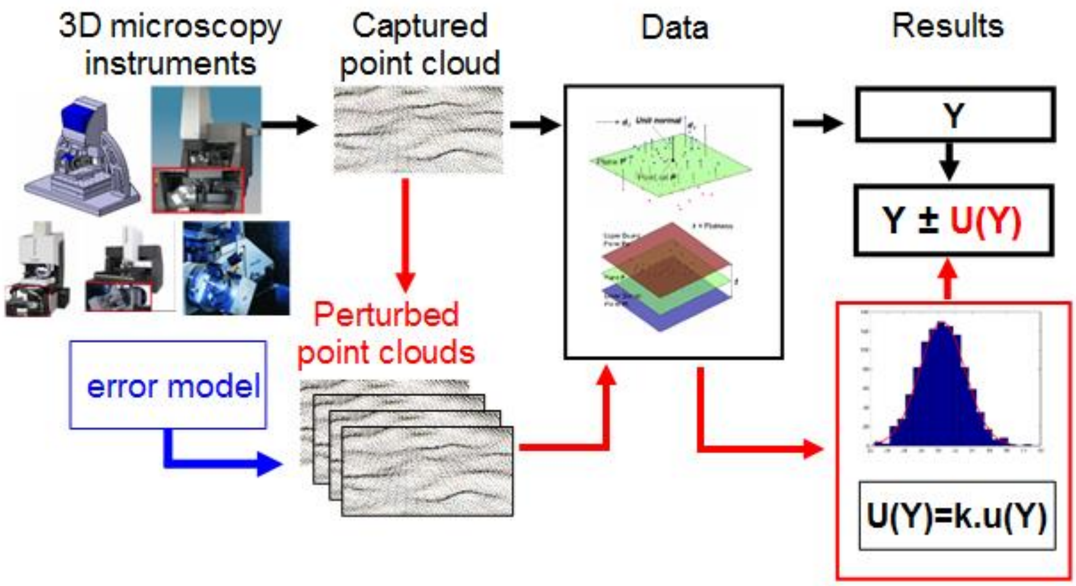

Figure 1: Framework a simulation method for the uncertainty estimate.

1.3 Research aim

In this paper, a simulation-based approach considering spatial correlation among points is proposed. The proposed model does not directly take into consideration physical phenomena related to interactions between materials and light; rather the model includes the effect of the physical interaction between the materials and the light inside several uncertainty sources, e.g. material types, and parameters of the simulation.

There are several technical reasons behind this consideration. First, even if well-established physical models exist for the interaction between electromagnetic waves and matter, their application is numerically impractical to apply and to the degree of accuracy required for 3DM measurement simulation. In general, the intensity value on each single pixel is not completely independent of the others. Hence, a single ray coming to the complementary metal-oxide semiconductor (CMOS) sensor has some degree of correlation with its neighbor ray of light [15]. And finally, some techniques add an additional contribution to the correlation among points, as the optimization function allowing the identification of the coordinates of the single point is calculated considering the neighboring pixels, selected by a windowing process [15].

Hence, to empirically model this phenomenon, the basis of the methodology is a Gaussian process [16], in which data are randomly distributed according to a multivariate Gaussian distribution, whose covariance structure depends on the spatial distribution of points. The multivariate Gaussian process can capture and simulate the correlation among points.

This paper is structured as follows. Section 2 describes the mathematical model allowing the simulation of the correlated points. Section 3 introduces Focus Variation Microscopy (FVM) as technology considered for the validation of the approach, and then focuses on the estimation of the parameters required to run the simulation. Finally, section 4 validates both the model and the estimation of the parameters according to the ISO/TS 15530-4 standard.

2. Task-specific uncertainty estimation by simulation in 3DM

The proposed approach relies on a point perturbation process (an error simulator) adopting a Gaussian process model taking into account the correlation among points, as shown in Figure 1. A correlation means that the error behavior of a point depends on other points within a certain distance from it. The simulation approach (figure 1, blue box) uses a Gaussian process model completely defined by a variogram function, we call it “variogram error model”. The need of this kind of model arises from the how a 3DM measurement is taken. As explained in section 1.3, it is expected that the measurement errors of the single sampling points are not independent but correlated. An independent simulation of them could then lead to a simulation far from the reality. The use of a Gaussian process described by a variogram error model allows the simulation of non-independent measurement errors, coherently with the measurement method.

2.1 Mathematical model for the simulation of a perturbed cloud of points

The core of the uncertainty estimation by simulation is the model for the perturbation of the point cloud. In general, the perturbation of the cloud of points is given $\varepsilon_{\theta x}, \varepsilon_{\theta y}, \varepsilon_{\theta z}$, which are rotation errors with respect to *x*, *y* and *z* axes, and $\varepsilon_x, \varepsilon_y, \varepsilon_z$ i.e. linear errors along *x*, *y* and *z* directions, respectively. Once these perturbations have been generated for each point, $\mathbf{p}_i'$, the coordinates of a single perturbed point, can be generated from the original measured points $\mathbf{p}_i$, (both are expressed in homogeneous coordinates) by multiplying the measured points $\mathbf{p}_i$ time an error matrix, $\mathbf{T}_{err}$, that is:

$$\mathbf{p}_i' = \mathbf{T}_{err}\mathbf{p}_i = \begin{bmatrix} 1 & -\varepsilon_{\theta z} & \varepsilon_{\theta y} & \varepsilon_x \\ \varepsilon_{\theta z} & 1 & -\varepsilon_{\theta x} & \varepsilon_y \\ -\varepsilon_{\theta y} & \varepsilon_{\theta x} & 1 & \varepsilon_z \\ 0 & 0 & 0 & 1 \end{bmatrix} \mathbf{p}_i \qquad (1)$$

In 3DM most of the error terms can be neglected. In fact, the *x* and *y* coordinates are not directly measured, but considered at their nominal value, as defined by the objective lens magnification and the sensor size of the 3DM. Moreover, during the scan the *x* and *y* do not move, and the translation along *z* is very small, so rotation errors are negligible. As such, the model can be simplified considering only the ε_z term.

A correlated error for the *i*-th point, ε_{zi}, is generated by sampling from a multi-variate Gaussian distribution. The multivariate normal distribution density function is formulated as:

$$f(\mathbf{p},\boldsymbol{\mu},\boldsymbol{\Sigma}) = \frac{1}{\sqrt{|\boldsymbol{\Sigma}|(2\pi)^m}} e^{-\frac{1}{2}(\mathbf{p}-\boldsymbol{\mu})\boldsymbol{\Sigma}^{-1}(\mathbf{p}-\boldsymbol{\mu})} \qquad (2)$$

where *m* is the dimension of the multivariate, i.e. the number of points, $\mathbf{p}$ represents the random vector with mean $\boldsymbol{\mu}$ and $\boldsymbol{\Sigma}$ is a $m \times m$ variance-covariance matrix which represents correlation. As the cloud of points is being randomly perturbed, the $\boldsymbol{\mu}$ term is set equal to 0. There are several ways of modelling $\boldsymbol{\Sigma}$. Among the others, we have selected the use of the variogram $2\gamma(\bullet)$ [16]. The variogram is well known and widely applied in spatial statistics, as its estimation is more robust compared to competitor method. The variogram function, together with the mean vector $\boldsymbol{\mu}$, fully characterizes the Gaussian process. Here we will address only isotropic homogeneous variogram function, as they are the simplest type of variograms, to simplify the discussion. Moreover, they have been found to be adequate for our case study. Details on non-isotropic homogeneous variograms can be found in the proposed literature. An isotropic homogeneous variogram function is defined as:

$$2\gamma(\mathbf{x}_1,\mathbf{x}_2) = 2\gamma(h) = E[(Z(\mathbf{x}_1) - Z(\mathbf{x}_2))^2] \qquad (3)$$

where $2\gamma(\bullet)$ is the variogram function, h is the lag (distance) between the generic locations $\mathbf{x}_1$ and $\mathbf{x}_2$, and $Z(\mathbf{x})$ is a response function at $\mathbf{x}$ (in 3DM the z-coordinate of a point). Please note that the assumption $2\gamma(\mathbf{x}_1,\mathbf{x}_2) = 2\gamma(h)$ implies the variogram is isotropic. The typical shape of a $\gamma(\bullet)$ function is illustrated in Figure 2. Example functions suitable to model isotropic homogeneous variogram models, but many more exist in literature, are:

$$\gamma(h) = \begin{cases} 0 & h = 0 \\ \mathrm{n} + \mathrm{s}\left(1\text{-}\exp\left(\text{-}3\dfrac{h^2}{\mathrm{r}^2}\right)\right) & h \neq 0 \end{cases} \quad \text{Gaussian model}$$

$$\gamma(h) = \begin{cases} 0 & h = 0 \\ \mathrm{n} + \mathrm{s}\left(1\text{-}\exp\left(\text{-}3\dfrac{h}{\mathrm{r}}\right)\right) & h \neq 0 \end{cases} \quad \text{Exponential model} \qquad (4)$$

$$\gamma(h) = \begin{cases} 0 & h = 0 \\ \mathrm{n} + \mathrm{s}\left(1\text{-}\exp\left(\text{-}3\dfrac{h}{\mathrm{r}}\right)\right) & 0 < h \leq \mathrm{r} \\ \mathrm{n} + \mathrm{s} & h \geq \mathrm{r} \end{cases} \quad \text{Spherical model}$$

where s, n, r are a sill, nugget, and range, respectively. These three parameters characterize all variogram models (Figure 2). Nugget (n) is a non-zero limit representing a discontinuity in a variogram origin. The nugget represents the pure white noise included in the random error. Sill (s) quantifies the error dispersion at infinite distance, i.e. global correlated and uncorrelated measurement noise. Range (r) is a measure of the distance up to which the measurement noise is significantly correlated.

Supposing the variogram error model and its parameters are known, having defined a set of locations $\mathbf{x}$, the $\mathbf{\Sigma}$ matrix can be built as

$$\Sigma_{ij} = s - \gamma(\mathbf{x}_i, \mathbf{x}_j) \qquad (5)$$

Once the $\mathbf{\Sigma}$ matrix is known any multi-normal random number generator can be applied to generate the ε_{zi} term at the $\mathbf{x}_i$ location.

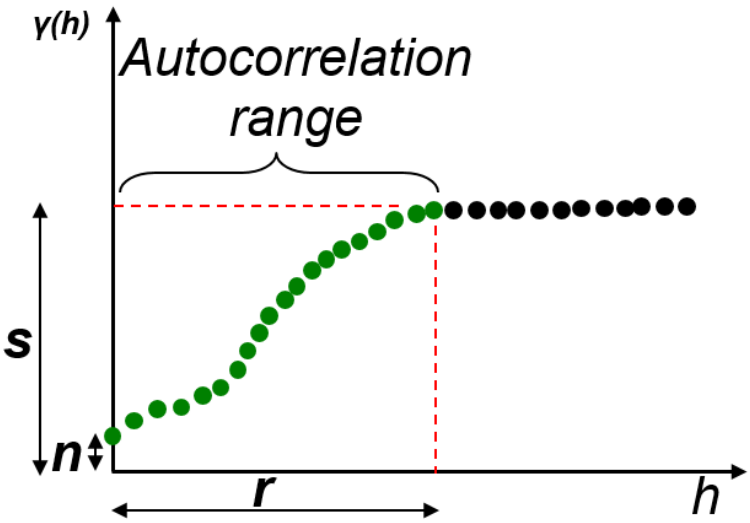

Figure 2: Illustration of variogram function and its s, r, n parameters.

2.2 Estimation of the variogram parameters for the simulation

The variogram model and its parameters need experimental identifications and evaluations. From experimental data, a least-square method is usually adopted to fit the empirical model of the variogram. Given a set of observations $Z(\mathbf{x}_i)$ (e.g. a single scan of a surface by 3DM), the value of the variogram at distance h can be estimated as

$$\hat{\gamma}(h) = \frac{1}{2|N(h)|}\sum_{N(h)}\left(Z(\mathbf{x}_i) - Z(\mathbf{x}_j)\right)^2 \qquad (6)$$

$$N(h) = \{(\mathbf{x}_i, \mathbf{x}_j) | \|\mathbf{x}_i - \mathbf{x}_j\| = h\} \qquad (7)$$

In the specific case of 3DM, as the points are locate on an evenly spaced grid, the possible values of h are well defined, so there are a series of well-defined values of $\hat{\gamma}(h)$. The $\hat{\gamma}(h)$ are then fitted, considering different variogram models. Based on R^2 of the least-square fitting, the best-fitted variogram model is selected, and then, the n, s, and r parameters are estimated.

The least square estimation of the s, n, and r parameters is in general applicable to a single sampled surface. It is then evident that the resulting parameters will be specific for the particular condition at which the scan has been conducted, e.g. material type. To have parameters that can be applied in a larger variety of conditions, we must modify them in order to take into account other uncertainty contributors. While the estimate of the nugget and the range can be properly estimated on a single scan, the sill, being representative of the overall variability of the measurement noise (correlated and uncorrelated), should include all the uncertainty contributors, and not only those from the condition at which it has been characterized so far. Hence, the parameter s resulting from the least square fitting shall be combined with other error sources before the simulation, according to the formula:

$$s_{sim} = \sqrt{s^2 + \sum s_i^2} \qquad (8)$$

where s is the sill originally obtained from the fitted model of the variogram and s_i is the contribution related with the i^{th} source of error. The estimate of the s_i terms require a deep analysis of the specific uncertainty sources affecting a particular 3D microscope, and an extensive experimental investigation of them. Anyway, once the contributors are known, their value can be extended to any future measurement.

3. Case study: the uncertainty estimation for a Focus Variation Microscope

Focus variation microscopy (FVM) is considered in this study as an example of 3DM. The FVM instrument used to demonstrate the proposed simulation approach is a 4^{th} generation FVM instrument by Alicona Imaging GmbH.

A FVM works based on the local focus condition of a stack of images taken at different distances from the measured surface to the FVM objective lens. The FVM working principle is as follows (see Figure 3): first, a stack of images is taken over a specified range of z-level (the distance from the measured surface to the scanning objective lens); the stack image acquisition is usually obtained by mechanically moving the objective lens of the FVM. For each z-level and for each pixel of the related stacked images, a focus value $F_z(x, y)$, which is a contrast of a pixel with respect to its neighboring pixels, is calculated. In most cases, the more the image is in focus, the higher the focus value is. For each pixel a mathematical fitting procedure is applied to the calculated focus values at each level, and the detected *z*-coordinate of a point is determined corresponding to the *z*-level with the highest $F_z(x, y)$ [15].

One fundamental advantage of a FVM instrument compared to other optical microscopy is its large working volume and its long working distance of the objective lens. This fundamental advantage provides the possibility of measuring the geometrical properties of a part.

The FV values calculated for each (*i*,*j*) pixel locations are obtained by comparing its contrast with respect to the intensity of its neighbor pixels.

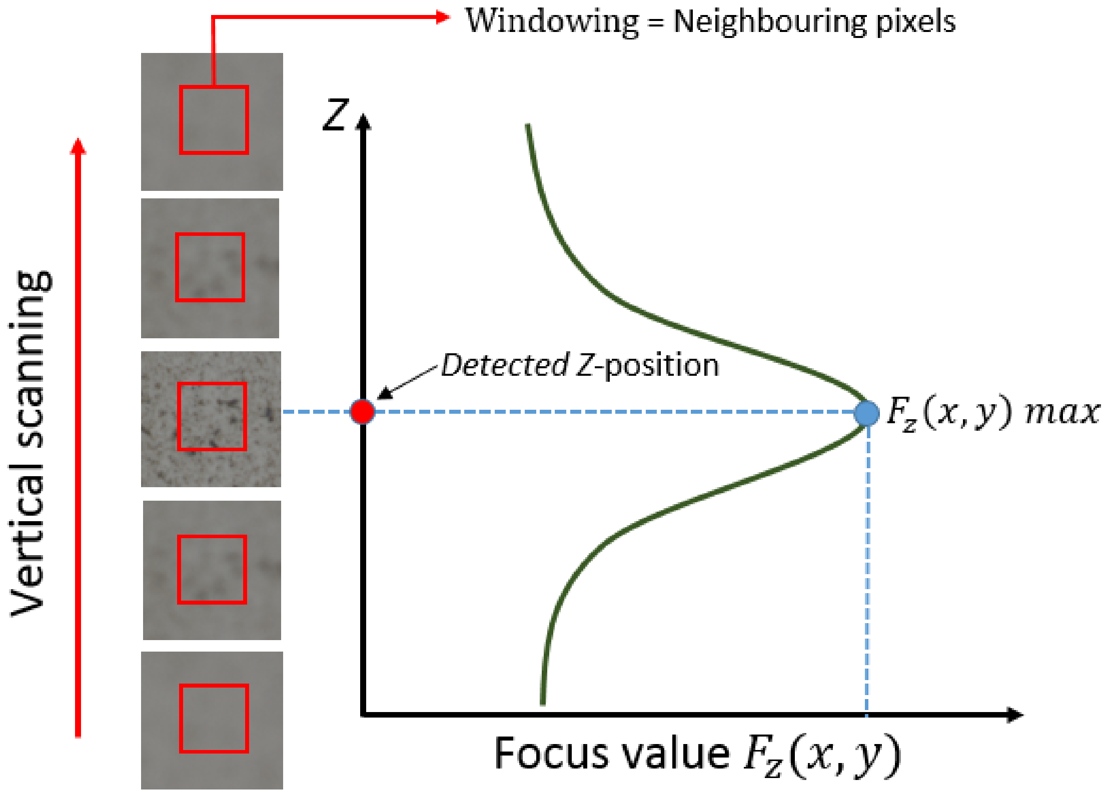

Figure 3: FVM working principle by calculating a focus value inside a windowing area.

3.1. Estimation of the variogram parameters

Different materials can be characterized by different variograms. In this study, we consider calibrated plates in aluminum (Al), stainless steel (SS), and titanium (Ti) for the variogram characterizations. It is worth to note that the variogram characterization data need to be obtained from a real surface in order to take into account the physical properties of the real measured surface, e.g. a roughness effect, local slope effect, reflectance effect, measurement angle effect and speckle noise effect of the surface to be included into the simulation process. Hence the variogram model takes into account the material type as uncertainty source. The variogram data from the actual surface measurements from the mentioned three materials will be used for uncertainty estimation with industrial case studies (section 4).

The variogram characterization, required to estimate the degree of a spatial correlation among points, is a fast procedure. The procedure only takes one single measurement with a single image field of a surface to be measured. It is worth noting that from a single image, a total of ~ one million points are obtained. A single image is sufficient to characterize the variogram because in an empirical variogram estimate every couple of points counts as a variance estimate replica.

The flatness of the three materials was calibrated by means of a traceable CMM with $E_{0,MPE}$=2+L/300 µm. Methods selected for the calibration are multi-position and multi-measurement strategies. A total of four different positions for the part were considered during the calibration of the plates. For each position, five measurements were repeated. By this method, an uncertainty contribution of the volumetric error of the CMM is also taken into account in the total calibration uncertainty. The results of the calibration and their uncertainty are (notation is based on GUM [4]): aluminum = 25.1(8) µm, stainless steel = 4.8(1) µm, and titanium = 4.1(2) µm.

To yield the data on which to define the variogram models, the plates were measured having the optical axis of the FVM approximately perpendicular to the plate itself, using the scan parameters in Table 1. The empirical variogram was then evaluated on these scanned surfaces. The variogram models in Eq. 4 are least-square fitted and the parameters *s*, *n*, and *r* are calculated. The model is selected based on the highest R^2 value of the data fitting. Table 2 presents the selected variogram models and their R^2 value for the considered three materials (Al, SS, Ti). Detailed variogram characterizations can be found in [17]. The nugget effect has been indicated equal to 0 because its value did not differ significantly from 0. This indicates a very strong statistical correlation among measurement errors at short distances, which is due to the FVM measurement principle based on a focus value calculated over a small patch of pixels.

Regarding the vertical and lateral resolution, they are set following the default values proposed by the instrument manufacturer with a 5× objective lens. It is worth noting that the selected lateral resolution is larger than the pixel size of the instrument. For the 5× objective lens, the pixel size is 1.76 µm. But, the actual resolution (the smallest distance between two features that can be resolved) will be larger than the pixel size due to the working principle of the instrument. As the measuring principle of the instrument needs the consideration of a patch of pixels around the considered point to calculate the focus measure that defines the *z*-level of the point, the effective resolution is reduced by the averaging effect of the focus measure estimated on the patch (see figure 3).

Table 1 Measurement parameter for Al, SS, and Ti materials.

Material	Exposure time [µs]	Contrast	Vertical Resolution [µm]	Lateral Resolution [µm]
Aluminum	114.4	1.33	0.4	7.82
Stainless steel	116.4	1	0.4	7.82
Titanium	224	1	0.4	7.82

Table 2 Selected variogram model for Al, SS and Ti.

Material	Variogram model	R^2	*s* [µm]	*n* [µm]	*r* [µm]
Aluminum (Al)	Exponential	0.56	31	0	114
Stainless steel (SS)	Exponential	0.78	2.8	0	56
Titanium (Ti)	Gaussian	0.71	3.9	0	18

3.2. Estimation of the contributors to the sill value for the simulation

An extensive experimental campaign was carried out to estimate the various s_i terms involved in FVM measurements. Therefore, the physical aspects of a FVM measurement, considered as uncertainty sources, are included into the simulation.

A FVM uses a sensor to take a series of images at different distances from a surface. A focus value is then calculated and a height is associate to each pixel. In case, stitching can be applied to increase the size of the scan. This process is prone to a lot of uncertainty sources that cannot be considered by the experiment proposed in section 3.1. Therefore, more uncertainty sources are estimated. Figure 4 schematically depicts the main uncertainty contributors in FVM measurements.

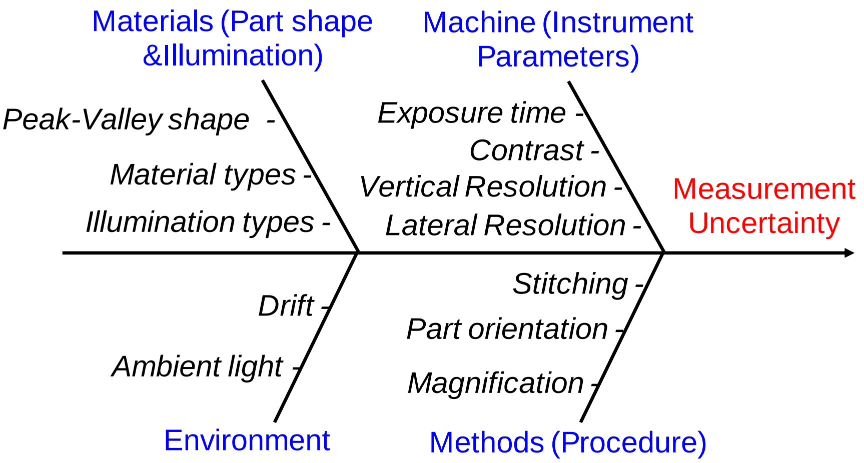

Figure 4: Diagram of the uncertainty contributors in FVM measurements [17].

An extensive experimental campaign has been conducted to study and quantify the effect of the mentioned factors and to include them into the simulation parameters. The three materials already mentioned were considered: aluminum (Al, specular surface), stainless steel (SS, lambertian surface), and titanium (Ti, lambertian surface). The numbers of points produced by a FVM measurement ranges from ~1 to ~4 million 3D spatial points. The analysis of variance (ANOVA) has been used to determine the significance of the factors.

Outliers were removed from the obtained datasets before measurement results could be extracted. This procedure is important since a large data point set is obtained from a single measurement cycle and outlying points among these (points presenting a very large algebraic deviation compared to other points in the scan) could reduce the accuracy of the measurement result. A simple outliers removal procedure has been applied, i.e. points having a deviation greater than 3σ from the fitting plane or cylinder of data points (depending on measured form) were removed, where σ is the sample standard deviation of all point deviations, that are distances from points to the fitted geometry.

A Shapiro-Wilk test, applied to the residuals (errors) of measured points, proved normality of the deviations with *p*-value around 0.8 for all the datasets. Figure 5 shows the histogram of the deviations (residuals) of points to the fitted plane for the three materials. The red line is the fitted Gaussian density function. The standard deviation (σ) of the residuals is presented in Table 3.

In this uncertainty characterization studies, the standard deviation σ of measurement residuals due to different parameters and measurement conditions is considered as parameter characterizing the impact or effect on the measurement uncertainty. The measurement residuals are σ of point deviations (a point distance error) to a fitted geometry, e.g. a plane, sphere and cylinder.

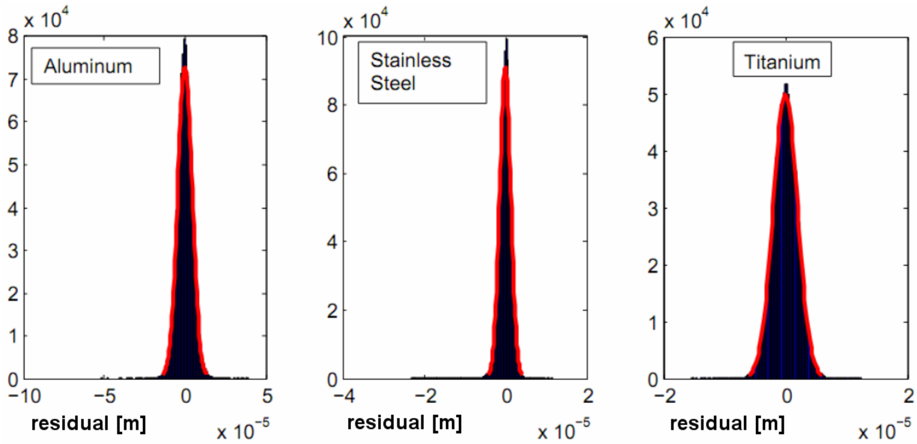

Figure 5: Histogram of residual from a fitted plane for the Aluminum, Stainless steel and Titanium materials.

Table 3 Standard deviation of residuals for the three materials.

Material	σ [μm]
Aluminum (Al)	4.49
Stainless steel (SS)	1.37
Titanium (Ti)	2.00

3.2.1 Influence of ambient light and different magnification lenses

A randomly structured surface of a polymeric injection-molded part was used to evaluate this contribution. The polymeric surface is considered because it has a high surface diffusivity and low roughness < 200 nm. Therefore, the surface is smooth and good to estimate the measurement repeatability in the study and to understand the effect of ambient light in a FVM measurement.

Measurements were carried out at 5× and 10× magnifications, both with the ambient light switched on or off. Numbers of 20 repetitions were carried out with around ~1 million points in each measurement repetition. Figure 6a plots the sigma of the residuals obtained by measuring with different lens types and ambient illuminations. In this figure, there are two sections. The left section presents results obtained using the 5× lens in an illuminated or dark room, while the right section presents the result obtained using the 10× lens. The main effect and interaction plot between the objective lenses and ambient light are shown in figure 6b and 6c, respectively.

From the obtained results, it seems that no influence of the ambient light is present. The different magnification is significant instead. The σ of the residuals at 10× reduces to 2.8 μm from the 3.7 μm obtained at 5×. The interaction between magnifications and ambient light is found to be not statistically significant. The range of σ for the lighted and dark room is around 0.01 μm. Meanwhile for difference lenses (magnification factor), the range is around 1.3 μm.

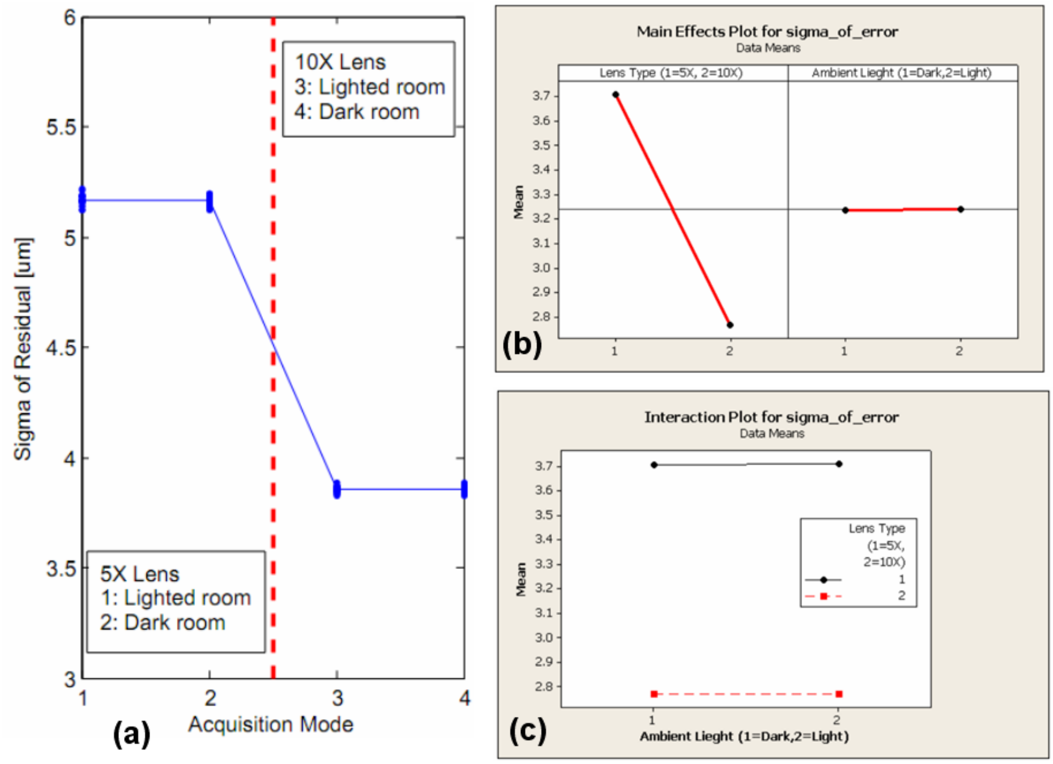

Figure 6: (a) Plot of sigma of residual obtained by different lenses and ambient light, (b) Main effect and (c) Interaction plot between the two factors.

3.2.2 Influence of different types of illumination

In this study, two materials were used, aluminum (specular) and random-structured polymer (lambertian) [18]. A 5× magnification was used. For each sample, 20 measurements were carried out (~1 million points each). The FVM instrument is equipped with three illuminators: axial-light, ring-light and polarized-light. From the analysis, different illuminations significantly affect σ.

From figure 7, for the aluminum surface (specular) the difference of σ from ring-light to polarized light reduces by about 0.6 µm, while for the polymer one, it increases by about 0.45 µm. Furthermore, the σ has inverse behavior when moving from specular to lambertian surface. Note that the plot of σ for the lambertian surface is only for ring light and polarized light since the surface cannot be captured with the axial light. The range of σ the different types of illumination with lambert surface is around 0.5 µm and with specular surface is around 1 µm.

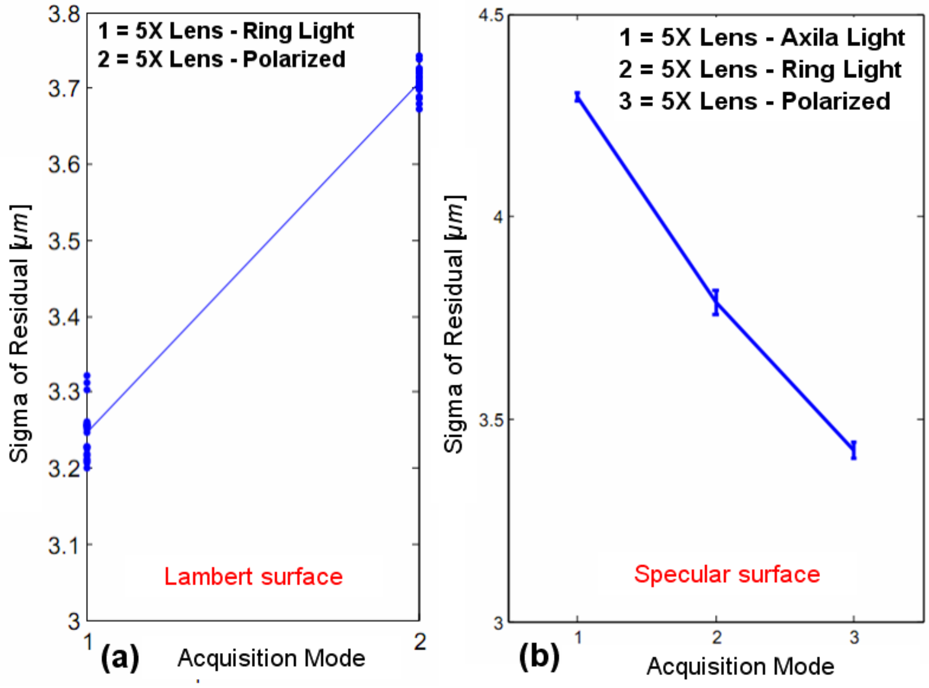

Figure 7: Effect of different illuminations for (a) Lambert surface and (b) Specular surface.

3.2.3 Influence of part orientations (surface slopes)

The three flat samples made respectively of aluminum, stainless steel, and titanium with the addition of coated steel (lambertian) and steel (specular) were used. The measurements were carried out for four different positions and steepness/slope orientations (0^0, 5^0, 10^0, 15^0). There are four position types which are combinations of two types of sample placement directions (along *x*-axis/horizontal or along *y*-axis/vertical) and two types of rotation directions (clockwise or anti-clockwise). Five measurement repetitions were carried out using the 5× objective lens, so in total 80 measurements were carried out for each material.

From the analysis, it is found that these factors significantly affect the σ. The range of σ for different types of measurement for aluminum, stainless steel and titanium varies around 2.5 µm, 2 µm and 1 µm, respectively. Figure 8 shows the plot of σ for each experiment as well as the measurement process (position and tilt/orientation direction). Figure 8 shows the plot of σ for different positions and different degrees of steepness (orientation). Note that for steel there are no data when the steepness is higher than 5^0 due to the specular reflectivity of the steel material, which causes the measurement to fail. The range of σ for the part orientation is around 3 µm considering the highest range value observed is for aluminum-ring light (figure 8 right: blue line).

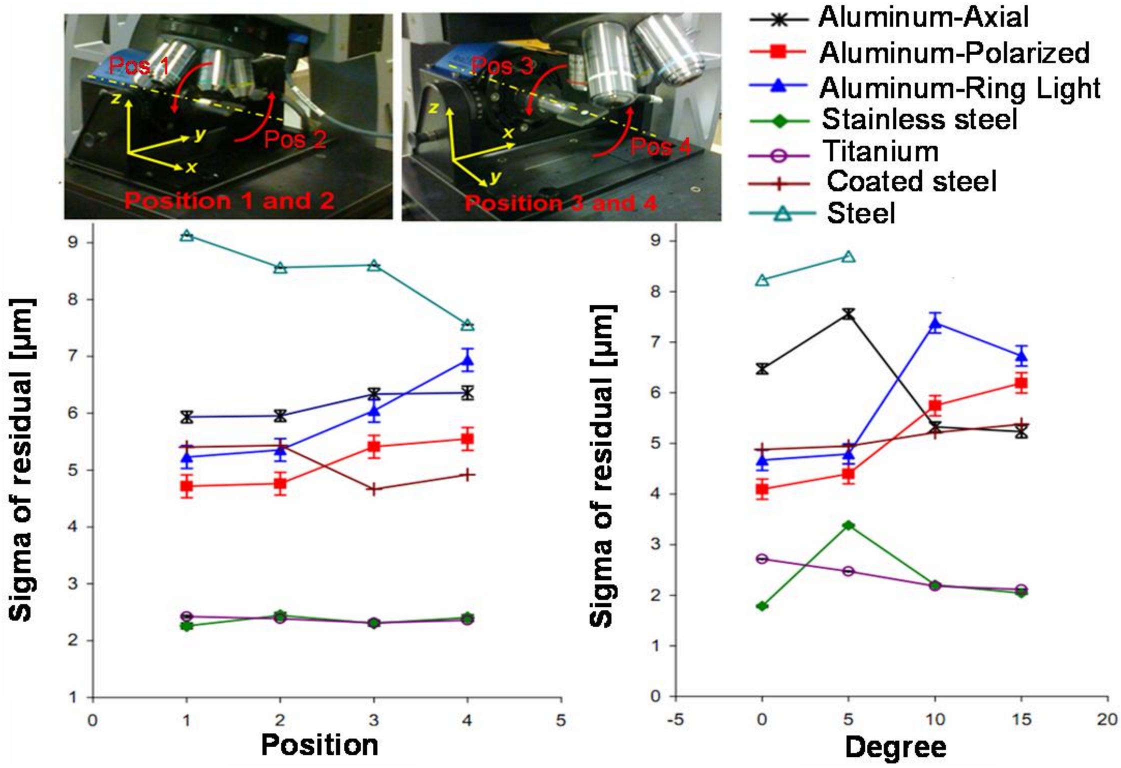

Figure 8: Results of σ for part orientation experiments.

3.2.4 Influence of peak-valley shape measurements

A machined part having peak and valley features (saw-tooth), made of glazed aluminum with grey color (lambertian), has been used. The edge of the machined part (either peak or valley) was measured 50 times. Each measurement generated about 45000 points. The σ in this case is the standard deviation of the distance of a point to a fitted 3D line representing an edge feature. The results show a statistically significant difference of σ between the two different shapes. The σ of peak measurement is lower by about 1.5 µm with respect to the valley one. The peak-valley measurement and the obtained σ are shown in figure 9. The range of σ for the peak-valley shape contributor is around 2.2 µm (by neglecting some outliers points in figure 9).

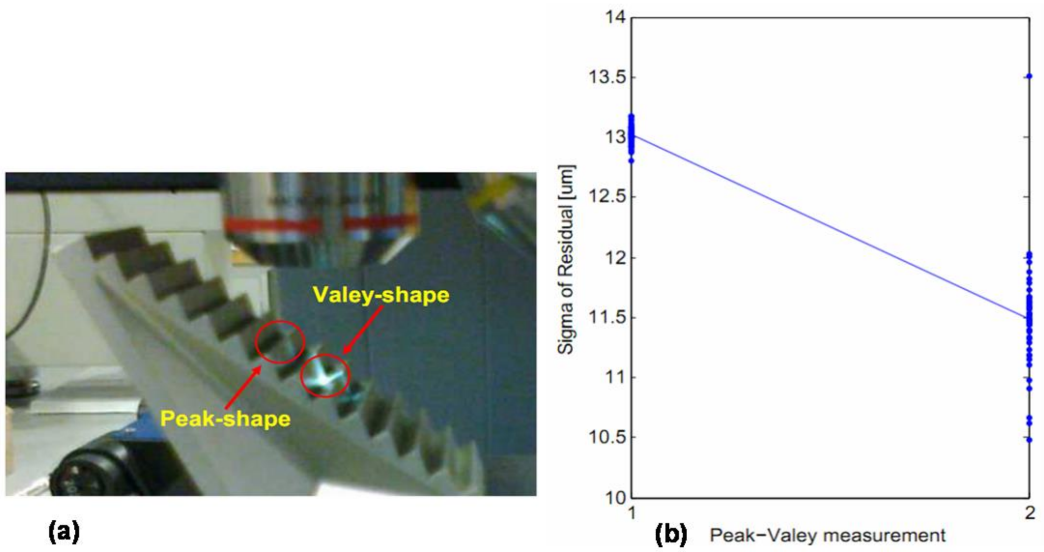

Figure 9: (a) Peak-valley measurement and (b) Obtained σ of residual.

3.2.5 *Stitching/no-stitching measurements*

Two types of sphere measurement were carried out: a single image (no-stitching) and four multiple images measurements. The measured part is an ISO 3290-1 steel sphere [19]. Numbers of 50 measurement repetitions were carried out generating ~750000 points per scan for a single image measurements and ~ 3250000 points for multiple ones. Table 4 provides details of the results of a point repeatability. The point is derived from the center of a fitted sphere to the obtained points.

The results show that the σ, in *x*-, *y*- and *z*-direction, of measurements by stitching are two times lower than the one without stitching. Hence, by stitching procedure, there is an averaging effect to the calculated position of the obtained points which suppresses part of the random error. Form errors in table 4 are the minimum distance between two concentric spheres covering all the obtained points. The range of σ for the stitching of multiple image measurements is around 0.9 µm.

Table 4: Repeatability of a single point.

Measurement type	**Form Error** /µm	
	Mean	Sigma (σ)
Single image	13.27	2.39
Multiple images	13.5	1.45

3.2.6 *Influence of measurement parameters*

There are four main parameters of an FVM measurement: exposure time, contrast, vertical and lateral resolutions. These factors can be controlled by the user before the measurement is carried out. A flat sample made of titanium was used for the study. There are four considered levels for lateral and vertical resolution factors and three levels for exposure time and contrast factors. The range of the lateral and vertical resolutions is based on the resolution limit of a 5× objective lens used for the experiments. Conversely, the selected range for exposure time and contrast were based on the range in which a good scan of the surface can be obtained. Table 5 and Table 6 present details of the lateral-vertical study and brightness-exposure time study, respectively.

From the analysis of experiment for the lateral and vertical resolution factors, it is found that only the lateral resolution is significant. As it can be seen in figure 10, the lower the lateral resolution is, the smaller the σ is. Decimation of points for bigger lateral resolution could be the reason for the reduction of noise since there is an averaging effect in data processing algorithms. There is no interaction effect between lateral and vertical resolutions as it can be observed in figure 11.

These results can be applied in practice for geometric measurement, in particular form measurement. As stated by Evans [11] optical instruments have considerably larger noise compared to contact ones. As form measurement is very sensitive to noise a larger lateral resolution is preferable to suppress measurement noise. The range of σ for the lateral and vertical resolution are around 3 µm and 0.01 µm.

Table 5: Detail of lateral and vertical resolutions influence study.

Type	Level	Resolution	Lateral point distance [µm]	Number of obtained points	Replication
Lateral	1	Highest	1.75	~2000000	25
Lateral	2	Medium (default)	2.62	~1000000	25
Lateral	3	Medium to low	4.66	~300000	25
Lateral	4	Lowest	7.82	~100000	25
Vertical	1	Highest	2.62	~1000000	25
Vertical	2	Medium (default)	2.62	~1000000	25
Vertical	3	Medium to low	2.62	~1000000	25
Vertical	4	Lowest	2.62	~1000000	25

Table 6: Detail of brightness and contrast resolution influence study.

Type	Level	Classification	Value set	Lateral point distance [µm]	Number of obtained points	Replication
Exposure time	1	Highest	339 µs	1.75	~1000000	25
Exposure time	2	Medium (default)	240 µs	2.62	~1000000	25
Exposure time	4	Lowest	110 µs	7.82	~1000000	25
Contrast	1	Highest	1.5	2.62	~1000000	25
Contrast	2	Medium (default)	1	2.62	~1000000	25
Contrast	4	Lowest	0.5	2.62	~1000000	25

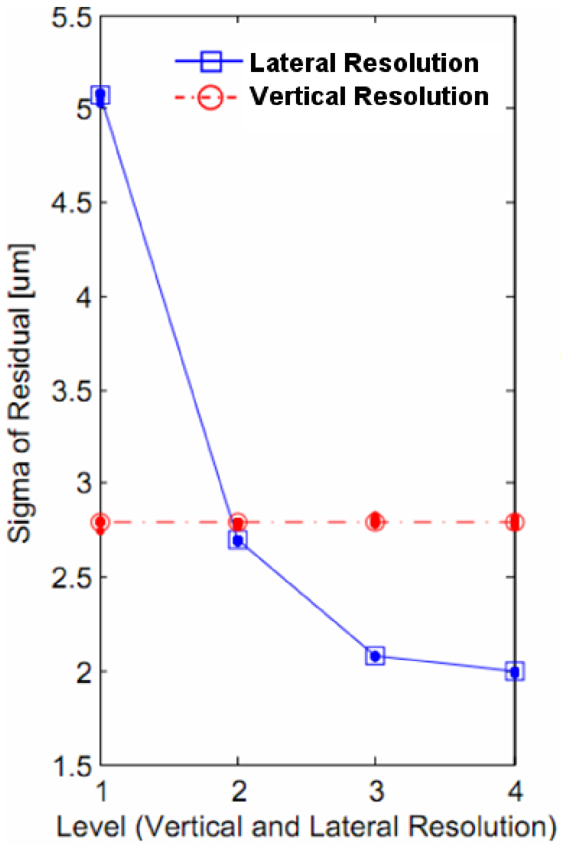

Figure 10: Effect of lateral and vertical resolutions.

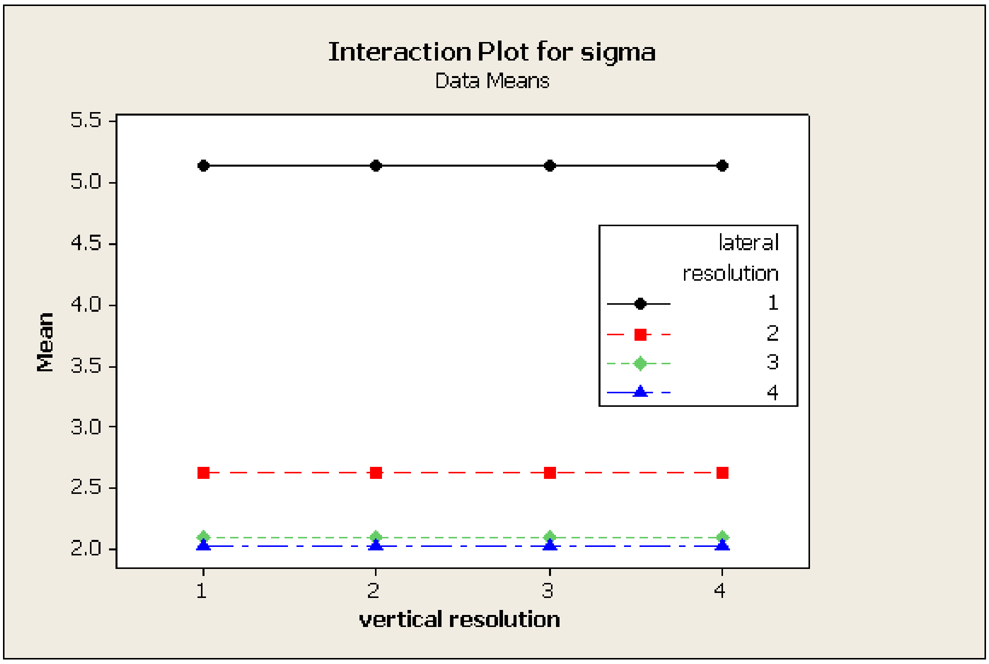

Figure 11: Interaction plot between lateral and vertical resolutions.

Exposure time (brightness) and contrast effects were then considered. From this analysis, it is shown that exposure time and contrast are significantly affecting the sigma of residual σ. Figure 12 shows that σ decreases when both exposure time and contrast are set to lower values. Interaction between exposure time and contrast is also found significant (figure 13). The range of σ for the contrast and exposure time settings are 0.2 µm and 0.3 µm, respectively.

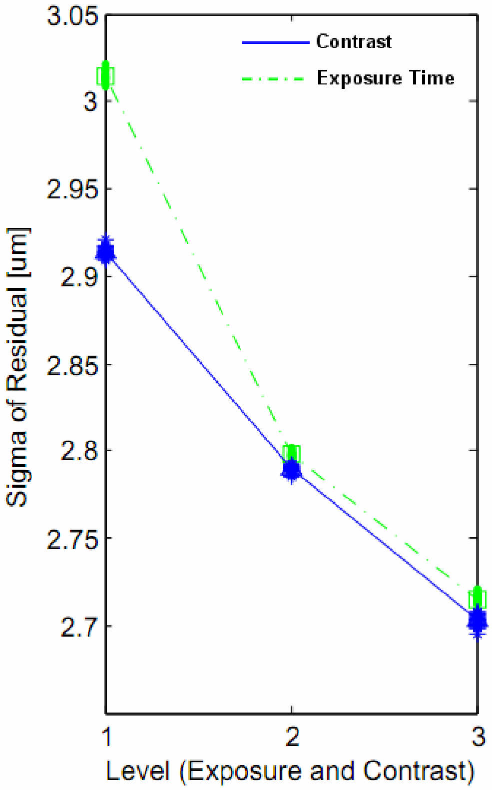

Figure 12: Effect of different levels of exposure time and contrast.

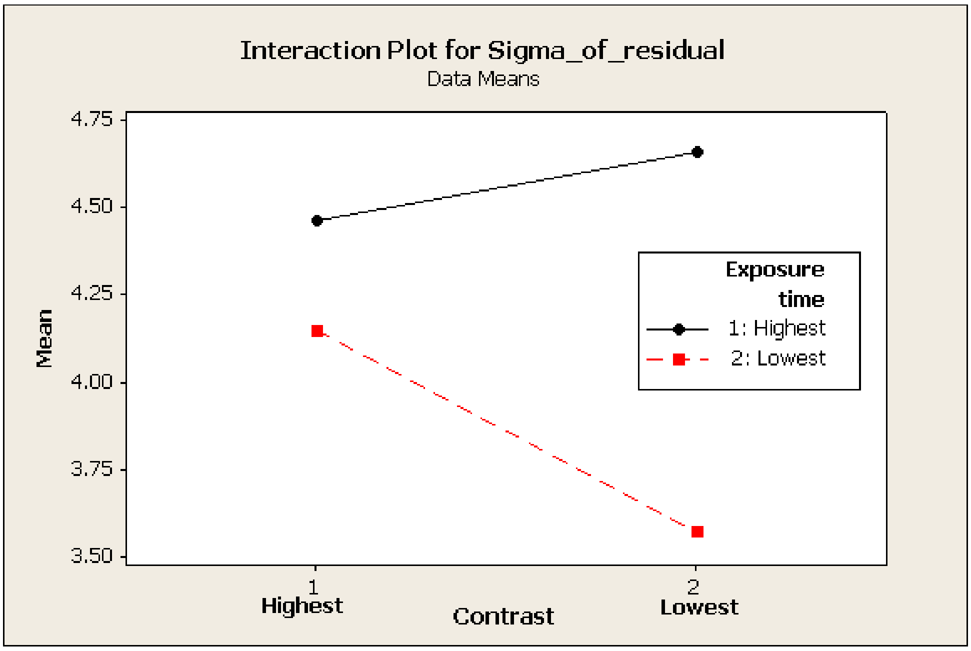

Figure 13: Interaction plot between the exposure time and contrast.

3.2.7 *Long measurement (drift) behaviors*

The variation of σ due to long measurement, both with and without stitching, has been investigated. Measurement time was considered because the FVM instrument components drift can be a relevant uncertainty source. The titanium flat sample has been used for measurements without stitching.

Measurements without stitching do not involve stage movements. Instead, for measurements with stitching from four images, an ISO 3290-1 steel sphere was used. The purpose of this type of measurements is to observe the behavior of the instrument in continuous measurement involving stage movements. Both types of measurements were carried out continuously without operator interventions. Thanks to a scripting ability of the instrument, this continuous measurement can be automatically run by the FVM instrument. The measurement used a 5× magnification lens with default lateral and vertical resolutions.

For non-stitching measurements, a total of 30 runs (~1 million points obtained for each measurement run) were carried out with a time span of around five hours. Sigma of residual σ and flatness are calculated for each measurement. Range of σ for this period of time is 0.0067 µm. Results of flatness measurements show a decreasing trend up to the 10th measurement sequence. The flatness interval (95%) for the first 100 minutes of measurement is 1.25 µm. After this 100 minutes period, the interval becomes 0.62 µm.

To represent a systematic error, measurements of distances from *i*-th plane to a reference plane (plane fitted from the first measurement) were conducted as can be seen from figure 14. In this figure, the systematic error representation is defined as the distance from the center point of the fitted plane of measurement *i* to the reference plane (plane fitted from the points of the first measurement). They show that the variation range (95%) of the distance during the first 19 measurements (the first 190 min.) is 0.16 µm, while after this period, it increases to 2.72 µm. Note that the value is shifted one position to the left, since the 1st measurement is not included. Starting from the 20th measurement, juggling phenomena of the measured distance to the reference plane of the flatness can be observed. These results are presented in figure 15.

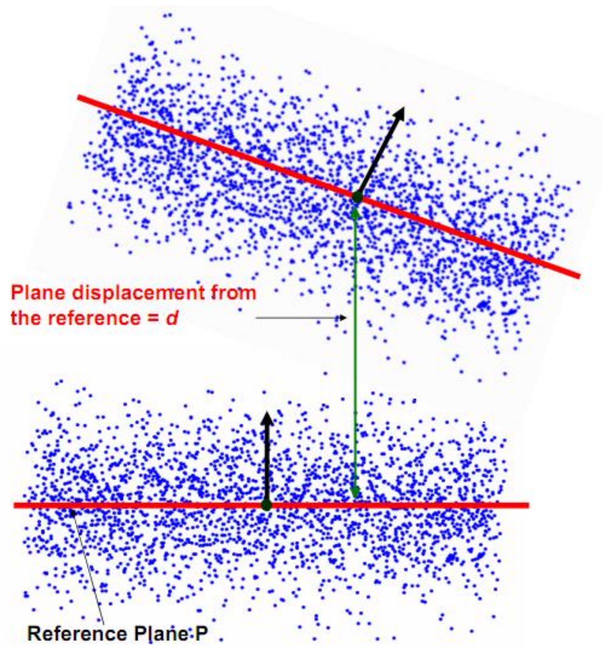

Figure 14: Illustration of distance to reference plane.

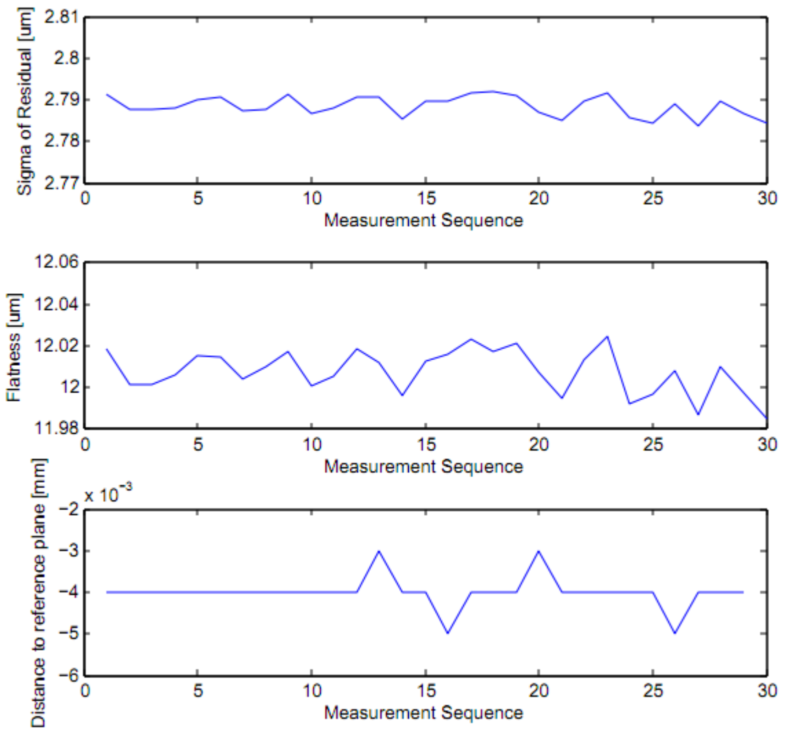

Figure 15: Long continuous measurement behaviors by plane measurements (without stitching).

Measurements of a sphere with stitching were carried out for 45 runs (~3 millions of points for each measurement run) which correspond to a six hour period. Parameters calculated from the measurement include sigma of the residuals σ, the distance of two consecutive centers and the sphere form error. The sigma of the residuals is used to represent a random error. For a systematic error representation, distances between two consecutive centers are calculated. A stable variation was observed during the first 40 measurements (the first 320 minutes). A shifting is observed for σ after 320 minutes is around 3 µm and for form error is about 40 µm, while the shift between the center distances is about 25 µm. Figure 16 presents the plot of the measurement drift behavior for this type of measurement. The range of σ for the drift is around 2 µm.

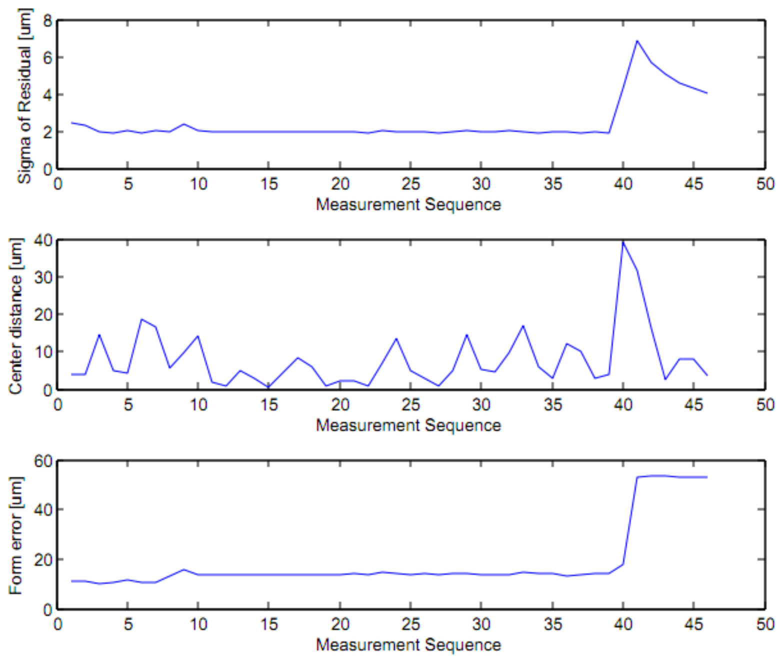

Figure 16: Long continuous measurement behavior by sphere measurements (with stitching).

3.3 Summary of the contributions

Finally, to summarize all the results from the uncertainty characterisation study, table 7 shows the range of the variation of σ for all the considered factors (worst-case scenarios). These values, that are considered relevant in each measurement task, are the s_i values included in the sill s_{sim} parameter used in the simulation model (equation 5).

Table 7: Summary of the influence of the factors.

Factor	Effect	σ [µm]
Peak-Valley shape	Significant	2.2
Illumination type with lambert surface	Significant	0.5
Illumination type with specular surface	Significant	1
Lateral Resolution	Significant	3
Vertical Resolution	Not Significant	0.01
Exposure time	Significant	0.3
Contrast	Significant	0.2
Stitching	Significant	0.9
Magnification	Significant	1.3
Part orientation	Significant	3
Drift	Significant	2
Ambient light	Not Significant	0.01

4. Validation

The ISO/TS 15530-4 standard [10] is the basis for the application and validation to guarantee the traceability of a simulation-based uncertainty estimation in coordinate metrology. As there are several deeply different coordinate measuring systems, the ISO/TS 15530-4 standard cannot define a general methodology for simulating the measurement and stating the uncertainty based on the simulation results. Instead, the ISO/TS 15530-4 standard defines the general requirements for the simulation, and the procedures for validating the uncertainty statements, thus guaranteeing the traceability.

The validation according to the ISO/TS 15530-4 standard includes both the mathematical model and the model parameters. The ISO/TS 15530-4 states that:

"*Performing a number of measurements on calibrated objects, the coverage of the uncertainty ranges is checked. The plausibility criterion should be satisfied for an appropriate percentage of the time (95% for k = 2); this criterion is that a statement of uncertainty is plausible if:* $|y - y_{cal}|/\sqrt{U_{cal}^2 + U^2} \leq 1$".

In this method, one should then calculate a E_n value for each measurement run. E_n is formulated as:

$$\mathrm{E_n} = |y - y_{\mathrm{cal}}| / \sqrt{U_{\mathrm{cal}}^2 + U^2} \qquad (9)$$

where y is a measurement result, y_{cal} is the calibrated value of y, U_{cal} is the expanded calibration uncertainty, and U is the expanded uncertainty obtained by simulation. If the expansion factor k is equal to 2, a good agreement can be concluded if approximately 95% of total measurements runs are characterized by $E_n < 1$.

Several case studies of geometric measurements are considered to validate the proposed simulation method; they include form (flatness measurements) and size measurements (diameter and height measurements). More complicated case studies can be found in [17]. It is worth to note that although the components are not a micro-sized component, the portion of features of the measured component and tolerances are at micro-scale [1, 2]. In the case study, the variogram model, used for uncertainty estimations by the proposed simulation, are selected based on the type of the material of the cased study considered.

4.1 Flatness measurement

The three calibrated samples originally adopted for the definition of the variogram models were considered (see §3.1). The simulation is applied to points obtained from a real measurement. Therefore, feature form deviation of the part is already included [20]. Figure 17 qualitatively shows that a variogram based simulation yields better results compared to a simulation of uncorrelated points. The red line shows the simulation result if the variogram model is applied: it is clear that it is close to the original data. Instead, if the noise is simulated as pure white noise with a standard deviation equal to the sill s of the variogram, the simulation result is far from the original data (green points).

Numbers of 100 flatness measurement runs were carried out by changing the part orientation (approximately perpendicular to the optical axis, 5° tilted clockwise and anticlockwise) to represent an orientation error when placing the part. The measurement parameters used followed those shown in Table 1 for each material type and orientation. To evaluate the uncertainty, 500 simulation runs were carried out. The sill s parameter of the simulation was modified according to Eq. (5) to consider the influence of the various uncertainty factors in the real measurement situation of the flatness measurement. Figure 18a shows results of the flatness measurements. It is worth noting that the flatness is based on a min-max fitting. This kind of fitting in general generates a non-Gaussian distribution of the measurement results.

The flatness samples were calibrated on a traceable tactile-CMM with $E_{0;MPE} = 2 + L/300$ µm where L is the measured length in mm (the CMM is periodically performance verified). The calibrations follows a multiple-measurements strategy that vary the position and orientation of the sample during the calibration process to take into account the volumetric error of the traceable tactile-CMM. Calibration results of the flat samples are $y_{cal} = 25.1$ µm and $U_{cal} = 1.6$ µm for Al, $y_{cal} = 4.8$ µm and $U_{cal} = 0.2$ µm for SS, and $y_{cal} = 4.1$ µm and $U_{cal} = 0.4$ µm for Ti. The estimated U for Al, SS, and Ti are 14.0 µm, 7.7 µm, and 10.1 µm, respectively. From calculation of each E_n value, the fraction of E_n values for which $E_n < 1$ for Al, SS, and Ti are 97%, 96%, and 98% respectively (Figure 18b), so the simulator can be considered validated in this case. From figure 18, some portions of E_n are larger than one. Having some portion of $E_n > 1$ suggest that the estimated uncertainty by the proposed simulation is not overestimating the expected uncertainty. Similar explanation for the E_n values are valid for all other presented case studies in this paper.

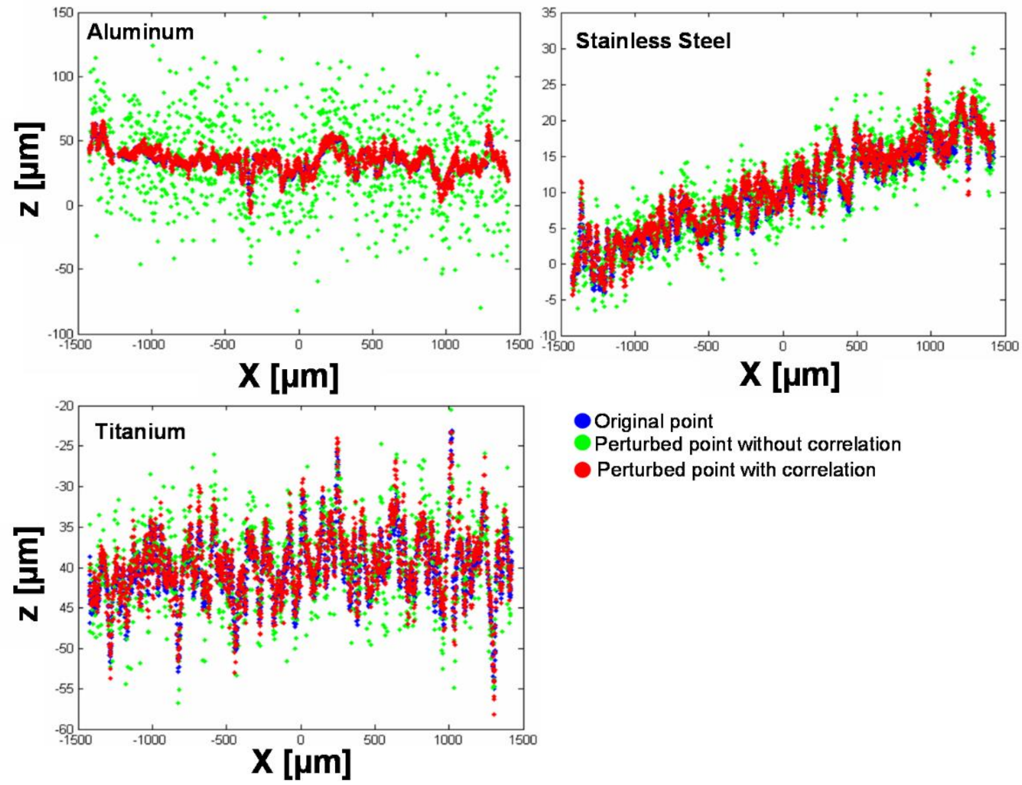

Figure 17: Plot of original points (blue) superimposed with the simulated points without considering (green) and with considering (red) the correlation among points for aluminum (Al), stainless steel (SS), and titanium (Ti).

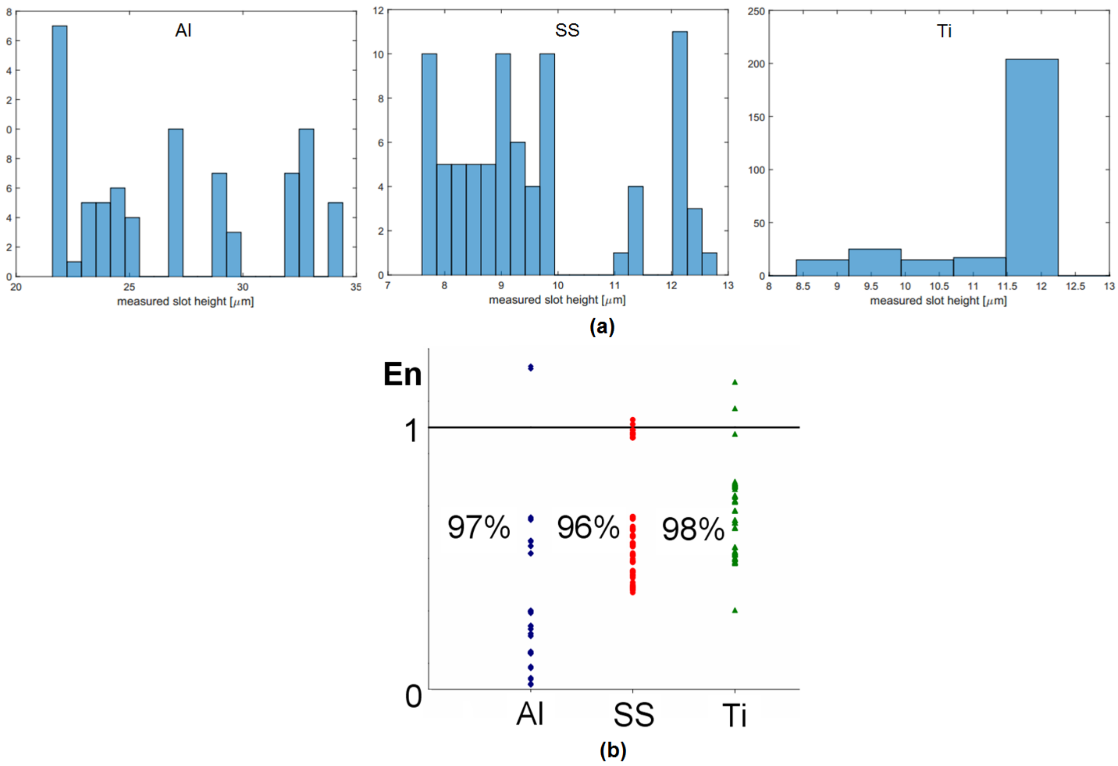

Figure 18: Plot of (a) histogram of the flatness value and (b) E_n values for the flatness measurement of Al, SS, and Ti.

4.2. Commercial micro-wire measurements

The measurement of a diameter (a dimensional characteristic) is presented in this case. An industrial micro steel wire with diameter of 310±2 µm was measured (Figure 19). The wire is used as a plug-gage to measure the nozzle diameter of a water jet machine. Since the part is a commercial plug-gage, y_{cal} and U_{cal} are based on the part's nominal specifications. The y_{cal} is considered to be equal to 310 µm. The U_{cal} of the plug-gage diameter is estimated as a type B uncertainty and is assumed to have a rectangular distribution. Hence, U_{cal} is equal to 2.31 µm.

Before running the simulation, the procedure, explained in Section 2, to determine the variogram model was carried out for steel since the variogram model of the steel material used in this case study has not yet been determined. The selected variogram model is a Gaussian one with *s*, *n*, and *r* parameters equal to 34.4 µm, 0 µm, and 14.8 µmm respectively. The estimated *U* is 5.6 µm obtained from 500 simulation runs *y*. A total of 85 measurement runs *y* were carried out with the following measurement parameters: 193.2 ms (exposure time), 0.44 (contrast), 0.6 µm (vertical res.) and 3.9 µm (lateral res.) by using 10× objective lens. From the E_n calculation, a total of 98 % values have $E_n < 1$, thus ensuring validation. The histogram of the measurement results *y* and the E_n calculation for each measurement are shown in figure 20. In figure 20 right, around 2 % of E_n values are more than one.

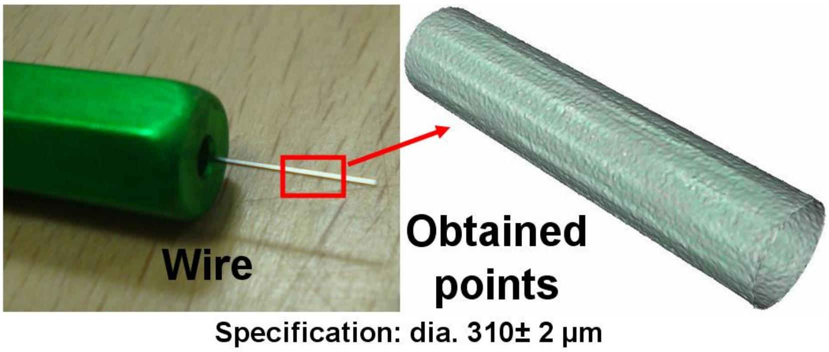

Figure 19: The micro-wire.

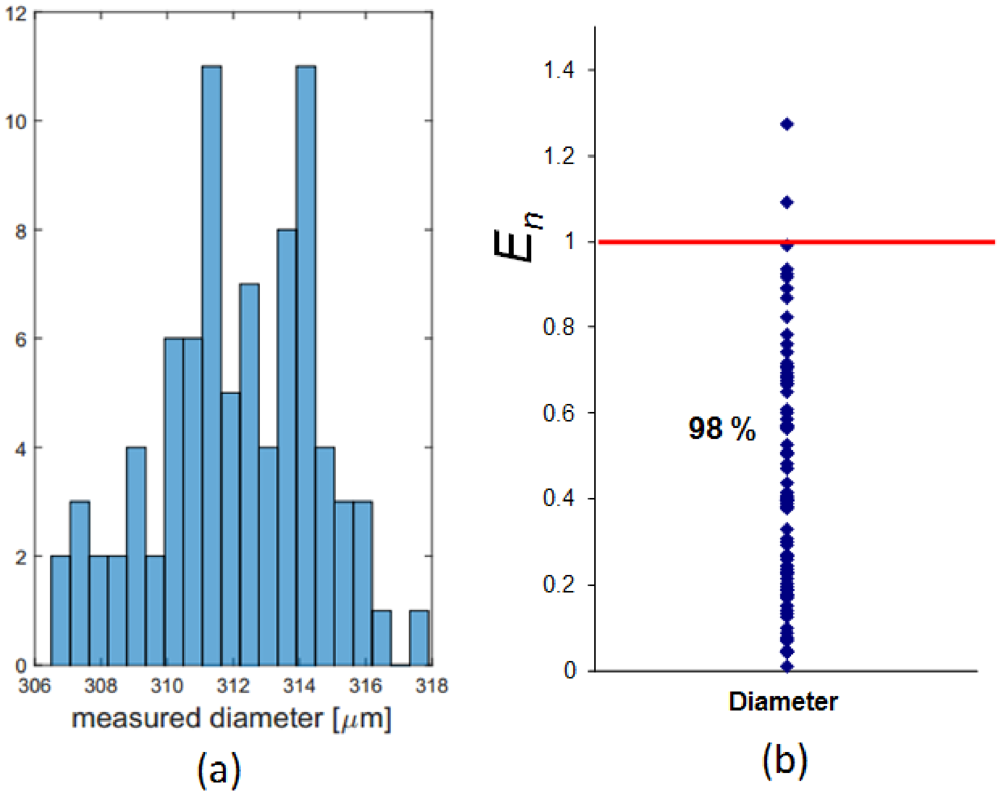

Figure 20: (a) Histogram of the diameter measurement results and (b) E_n values for the diameter measurement validation.

4.3. Step-height measurements of a slot-milled steel component

A measurement of the step-height of a slot-milled part is presented in this study. The part was made of a steel material by using a precision micro-milling machine. The part, the slot height definition and an example of the measured surface are shown in figure 21. Measurement parameters for the slot step-height measurement are exposure time = 88.32 µs, contrast = 0.2, lateral resolution = 7.83 µm and vertical resolution = 0.4 µm by using a 5× objective lens.

The results of a calibration process using a traceable tactile-CMM are y_{cal} = 698.7 µm and expanded uncertainty U_{cal} = 0.25 µm. Total of 100 measurements runs y was carried out. From around 500 simulations runs to estimate the uncertainty of the slot measurement, an expanded estimated uncertainty U is obtained as 0.45 µm. From a total of 100 measurement runs y, 93% (almost 95%) of E_n values are less than 1, hence the simulation and the uncertainty estimation are validated. Figure 22 shows the histogram of the measurement results and the E_n value calculation for each measurement.

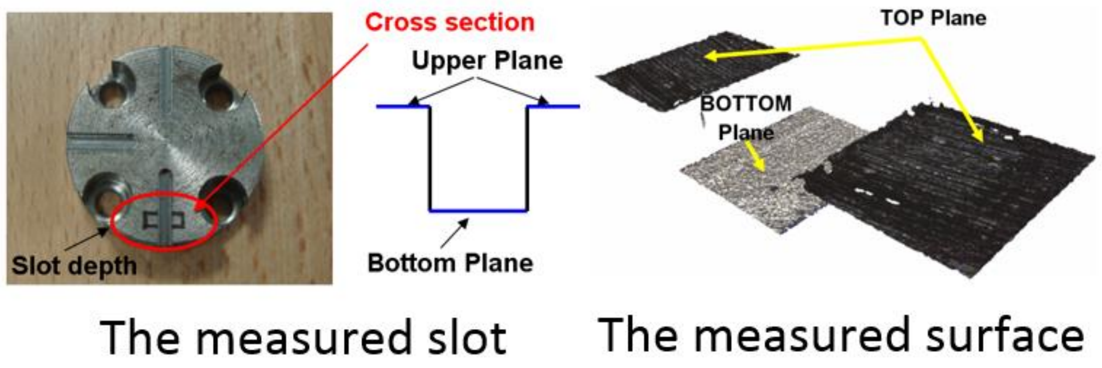

Figure 21: The measured slot and its obtained surface.

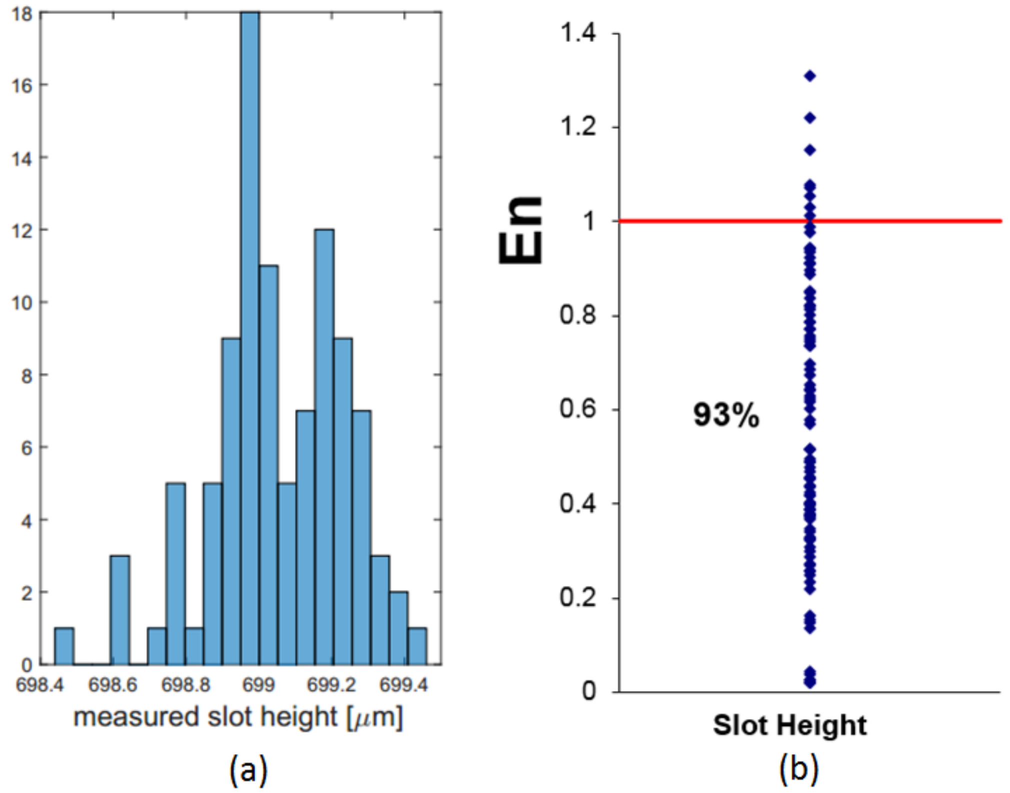

Figure 22: (a) Histogram of the height measurement results and (b) E_n values for the slot step-height measurement validation.

5. Conclusions

This paper presents a proposal of a simulation-based approach to estimate the task-specific measurement uncertainty of a 3DM performing geometric inspections. A case study regarding FVM is proposed. The case study is validated according to the ISO/TS 15530-4 standard. The method considers the correlation among points obtained by the optical instrument since correlation naturally occurs among points measured sequentially or continuously. Variogram models are determined for each material to represent the property of correlations among points. In general, the correct type of variogram (Gaussian, exponential, spherical, etc.) is defined based on the gathered experimental data. In this work, we are suggesting and describing a possible approach we developed and validated in a case study. The proposed approach can be applied to other type of 3DM instruments and can be implemented and integrated into instruments software system as a module.

Extensive uncertainty characterization has been carried out to identify and quantify the uncertainty sources and incorporate them into the simulation parameters. The validation is carried out with industrial case studies and the results show that the simulated uncertainties have a good agreement with the real measurement.

The proposed simulation approached can be summarised as follows:

1. Define the variogram model and quantify the s, n and r parameters for each material type. This step is carried out once for every different material.
2. Experimentally evaluate the additional uncertainty sources not considered in the variogram, but influencing the measurement result. The uncertainty sources quantification is carried out once for each type of instrument.
3. Measure the part to inspect, and compute the measured value y.
4. Having modified the value of s considering the additional sources of uncertainty, apply the variogram model to generate an adequate number of simulation runs and the related perturbed clouds of points, compute the simulated measured values and, based on these values, estimate the expanded uncertainty U.
5. State the measurement result $y \pm U$.

Further works include building a database of optimal variograms for various types of materials and applying the proposed method to estimate task-specific uncertainty for surface texture measurements.

Acknowledgements

Financial support to this work has been provided as part of the project REMS - Rete Lombarda di Eccellenza per la Meccanica Strumentale e Laboratorio Esteso, funded by Lombardy Region (Italy), CUP: D81J10000220005 and AMala – Advanced Manufacturing Laboratory, funded by Politecnico di Milano (Italy), CUP: D46D13000540005.

Acknowledgment is due to the Recruitment Program of High-end Foreign Experts of the Chinese State Administration of Foreign Experts Affairs.

References

[1] L. Alting, F. Kimura, H. Hansen, G. Bissacco, Micro engineering, CIRP Annals - Manufacturing Technology 52 (2) (2003) 635–657. doi:10.1016/S0007-8506(07)60208-X.

[2] H. Hansen, K. Carneiro, H. Haitjema, L. De Chiffre, Dimensional micro and nano metrology, CIRP Annals - Manufacturing Technology 55 (2) (2006) 721–743. doi:10.1016/j.cirp.2006.10.005.

[3] ISO/IEC, ISO/IEC GUIDE 99:2007(E/F): International vocabulary of metrology - basic and general concepts and associated terms (VIM) (2007).

[4] G. Moroni, S. Petrò, W. Syam, Four-axis micro measuring systems performance verification, CIRP Annals - Manufacturing Technology 63 (1) (2014) 485–488. doi:10.1016/j.cirp.2014.03.033.

[5] G. Moroni, W. Syam, S. Petrò, Performance verification of a 4-axis focus variation co-ordinate measuring system, IEEE Transactions on Instrumentation and Measurement 66 (1) (2017) 113–121. doi:10.1109/TIM.2016.2614753.

[6] ISO/IEC, ISO/IEC GUIDE 98-3: Uncertainty of measurement - Part 3: Guide to the expression of uncertainty in measurement (GUM:1995) (2008).

[7] R. Wilhelm, R. Hocken, H. Schwenke, Task specific uncertainty in coordinate measurement, CIRP Annals - Manufacturing Technology 50 (2) (2001) 553–563. doi:10.1016/S0007-8506(07)62995-3.
[8] G. Moroni, S. Petrò, Optimal inspection strategy planning for geometric tolerance verification, Precision Engineering 38 (1) (2014) 71–81. doi:10.1016/j.precisioneng.2013.07.006.
[9] International Organization for Standardization, ISO 15530-3: Geometrical Product Specifications (GPS) – Coordinate measuring machines (CMM): Technique for determining the uncertainty of measurement – Part 3: Use of calibrated workpieces or standards (2011).
[10] International Organization for Standardization, ISO/TS 15530-4: Geometrical Product Specifications (GPS) - Coordinate measuring machines (CMM): Technique for determining the uncertainty of measurement - Part 4: Evaluating task-specific measurement uncertainty using simulation - First Edition (Jun. 2008).
[11] C. Evans, Uncertainty evaluation for measurements of peak-to-valley surface form errors, CIRP Annals - Manufacturing Technology 57 (1) (2008) 509–512. doi:10.1016/j.cirp.2008.03.084.
[12] J.-P. Kruth, N. Van Gestel, P. Bleys, F. Welkenhuyzen, Uncertainty determination for cmms by monte carlo simulation integrating feature form deviations, CIRP Annals - Manufacturing Technology 58 (1) (2009) 463–466. doi:10.1016/j.cirp.2009.03.028.
[13] C. Cheung, M. Ren, L. Kong, D. Whitehouse, Modelling and analysis of uncertainty in the form characterization of ultra-precision freeform surfaces on coordinate measuring machines, CIRP Annals - Manufacturing Technology 63 (1) (2014) 481–484. doi:10.1016/j.cirp.2014.03.032.
[14] E. Trapet, F. Waeldele, The virtual CMM concept, in: P. Ciarlini, M. Cox, F. Pavese, D. Richter (Eds.), Advanced Mathematical Tools, II, World Conference Scientific, Singapore, 1996, pp. 238–247.
[15] R. Leach (Ed.), Optical Measurement of Surface Topography, Springer-Verlag, Berlin, Germany, 2011. doi:10.1007/978-3-642-12012-1.
[16] N. A. C. Cressie, Statistics for Spatial Data, 1st Edition, Wiley-Interscience, New York, 1993.
[17] W. P. Syam, www.politesi.polimi.it/handle/10589/100382Uncertainty evaluation and performance verification of a 3d geometric focus variation measurement, Ph.D. thesis, Politecnico di Milano, Milan, Italy (2015). www.politesi.polimi.it/handle/10589/100382
[18] D. A. Forsyth, J. Ponce, https://books.google.it/books?id=gM63QQAACAAJComputer Vision: A Modern Approach, Always learning, Pearson, 2012. https://books.google.it/-books?id=gM63QQAACAAJ
[19] International Organization for Standardization, ISO 3290-1: Rolling bearings – Balls – Part 1: Steel balls (2014).
[20] J. M. Baldwin, K. D. Summerhays, D. A. Campbell, R. P. Henke, Application of simulation software to coordinate measurement uncertainty evaluations, NCSLI Measure 2 (4) (2007) 40–52. doi:10.1080/19315775.2007.11721398.